Assessment of Castigliano's Theorem on the Analysis of Closing Loop for Canine Retraction by Experiment and Finite Element Method. Part II

Variddhi Ungbhakorn
Mahanakorn University of Technology, Nong Chok, Bangkok 10530, Thailand
Tel: (662) 218-6629
E-mail: fmevub@eng.chula.ac.th
Corresponding author

Varintra Ungbhakorn
Department of Orthodontics, Faculty of Dentistry
Chulalongkorn University, Bangkok, Thailand 10330
Tel: (662) 218-8754
E-mail: nchudhabuddhi@hotmail.com

Paiboon Techalertpaisarn
Department of Orthodontics, Faculty of Dentistry
Chulalongkorn University, Bangkok, Thailand 10330
Tel: (662) 218-8951
E-mail: gonggort2@hotmail.com

Abstract

The optimum configurations for canine retraction of four types of closing loops in Part I are used to study in Part II by FEM and experimental verification. The experimental results of loop stiffness and M/F presented by Siatkowski are also compared to those obtained from FEM. Acceptable agreement has, been demonstrated, hence, it is recommended that the results from FEM are used for actual estimates. Finally, the algebraic equations for loop stiffness and M/F of the vertical helical loop, T-loop and helical T-loop constructed from 0.40x0.55 mm stainless steel arch wire are presented as a function of the gable bend angle to facilitate orthodontists in the calculation of the gable bend angle to yield the required M/F and loop stiffness.

Keywords: closing loop, canine retraction, Castigliano's theorem, finite element method

1. Introduction

In part I of this article, the theoretical derivations for the expressions of M/F and loop stiffness, K, for four types of closing loops were presented in details. The optimum configurations were based on maximizing the inherent M/F of each loop type without gable bend. The total height and width of each configuration are limited to 10 millimeters for canine retraction. These optimum configurations are used for experimental verification of the loop stiffness in Part II. Since the essential assumptions for the Castigliano's theorem are violated, namely, small displacement, co-planar force system, and small distortion of closing loop shape after activation, large discrepancies to the experimental stiffness are expected. Therefore a theoretical analysis by FEM is used to calculate M/F and loop stiffness of every optimum configuration and the values of loop stiffness are then compared to those from experiments. Discrepancies of the results are within acceptable values, thus, we can have confidence in the values of M/F predicted by

FEM, with or without gable bends. Since the graphs of M/F and moments vs. gable bend angle, θ, are straight lines, we are able to derive the algebraic equations of M/F and moments as the function of the gable bend angle for each loop type at various activating forces ranging from 50 to 200 gm (0.49 to 1.96 N). These equations will be useful to orthodontists who have to select a gable bend angle to yield the desired value of M/F. Each optimum loop configuration used in this Part II study is as follows:

Vertical helical loop : R = 1.5 mm, H = 8.5 mm
T-loop : d = 0 mm, R = 1.0 mm, H = 8 mm, L = 4.0 mm
Helical T-loop : d = 0 mm, R = 1.0 mm, H = 8 mm, L = 4.0 mm
Opus90 loop : R = 1.0 mm, H = 8 mm, L = 8 mm

2. Materials and Methods

The experimental apparatus is the Lloyd universal testing machine LF plus with 10 Newton load cell. The samples of closing loops were constructed from 0.40x0.55 mm (0.16x0.22 inch) stainless steel arch wire. The four types of closing loops with the optimum configurations are shown in Fig. 1. The test run consisted of incremental loop activations at 0.50, 1.00, 1.50, 2.00, 2.50 and 3.00 mm. Each loop was set up at the center of inter-bracket distance (IBD). Five samples of each loop configuration were used for each test run. To confirm the repeatability of the experiment, all samples were kept for two weeks and the same test procedure was performed again. All results closely agree with the previous ones. Thus the reliability of all data points is assured. Example of statistical analysis of T-Loop data is obtained as follows:

Maximum stiffness = 60.77 gm/mm
Minimum stiffness = 58.17 gm/mm
Mean stiffness = 59.63 gm/mm
Standard deviation = 1.13
Standard error = 0.51
Coefficient of variation = 1.90 %

3. Results

3.1 Experimental findings

The shapes of each loop type before and after activation of 3 mm is shown in Figs. 2 to 5. All IBD's are equal to 14 mm. It is seen that the deformed configurations differ from the original configurations significantly. In an engineering aspect, this implies that the equilibrium force system of the deformed configuration rather than the unloaded configuration should be used in the analytical formulation in order to get a good prediction. This restriction is removed by using FEM. The comparison of the loop stiffness between those from Castigliano's theorem (K_C) and experiments (K_E) are shown in Table I and the discrepancies are large as expected.

Table I. Values of loop stiffness from Castigliano's theorem and experiments

Loop type	Loop stiffness (gm/mm)	
	K_C	K_E
Vertical helical loop	33.80	81.90
T-loop	23.80	59.63
Opus90 loop	19.60	55.94
Helical T-loop	23.50	47.66

3.2 Finite element results

The computer program used in finite element analysis is MSC/NASTRAN [1]. The numerical and graphical results for each loop type are presented below.

3.2.1 Vertical helical loop

Figs. 6 to 10 are the results from FEM of the optimum vertical helical loop. Fig. 6 shows the deformed shape of the loop without gable bend angle. It is noticed that the theoretical deformed shape resembles the experimental shape shown in Fig. 2 (b). Fig. 7 shows the finite element results for ratios of M/F using both small deflection and large deflection theories. It is seen that the difference in both theories is negligible, namely:
Small deflection M/F = 4.67 mm
Large deflection M/F = 4.64 mm

Fig. 8 shows the effect of gable bends on the loop stiffness. The stiffness increases as the gable bend angle increases. The effect of gable bend angle on the ratio of M/F is clearly demonstrated in Fig. 9 for various activating forces and their corresponding moments are shown in Fig. 10. Since graphs in Fig. 9 and 10 are straight lines, we can derive their algebraic equations for M/F and M as a function of gable bend angle in degrees as given in Table II and

III. If proven reliable for good estimates, these equations will be very useful for orthodontists.

Table II. Equations of M/F of vertical helical loop for any θ (degrees)

F (gm)	M/F (mm) Equations
50	M/F = 0.1759 (θ) + 4.67
100	M/F = 0.0925 (θ) + 4.67
150	M/F = 0.0648 (θ) + 4.67
200	M/F = 0.0509 (θ) + 4.67

Table III. Equations of moments of vertical helical loop for any θ (degrees)

F (gm)	M (gm.mm) Equations
50	M = 8.7932 (θ) + 230.12
100	M = 9.2518 (θ) + 464.16
150	M = 9.7163 (θ) + 698.20
200	M = 10.178 (θ) + 932.24

3.2.2T-loop

Since the finite element analysis of T-loop is similar to the vertical helical loop, results of T-loop corresponding to Figs. 7, 9 and 10 will be omitted. Fig. 11 shows the deformed configuration resembling the experiment shown in Fig. 3 (b). The ratio of M/F without gable bend is 5.06 mm. The effect of gable bend angles on the loop stiffness is demonstrated in Fig. 12. The algebraic equations for M/F and moments as the function of the gable bend angle in degree are given in Table IV and V.

Table IV Equations of M/F of T-loop for any θ (degrees)

F (gm)	M/F (mm) Equations
50	M/F = 0.1521 (θ) + 5.06
100	M/F = 0.0827 (θ) + 5.06
150	M/F = 0.0595 (θ) + 5.06
200	M/F = 0.0479 (θ) + 5.06

Table V. Equations of moment of T-loop for any θ (degrees)

F (gm)	M (gm.mm) Equations
50	M = 7.6047 (θ) + 250.05
100	M = 8.2653 (θ) + 503.34
150	M = 8.9259 (θ) + 756.63
200	M = 9.5867 (θ) + 1009.9

3.2.3 Helical T-loop

The deformed configuration of the helical T-loop resembles Fig. 5 (b) is shown in Fig. 13. Its M/F without gable bend is 5.82 mm. The loop stiffness depends on the gable bend angle as shown in Fig. 14. The algebraic equations for M/F and moments as a function of the gable bend angle in degrees are given in Table VI and VII.

Table VI. Equations of M/F of helical T-loop for any θ (degrees)

F (gm)	M/F (mm) Equations
50	M/F = 0.0934 (θ) + 5.82
100	M/F = 0.0509 (θ) + 5.82
150	M/F = 0.0367 (θ) + 5.82
200	M/F = 0.0296 (θ) + 5.82

Table VII. Equations of moments of helical T-loop for any θ (degrees)

F (gm)	M (gm.mm) Equations
50	M = 4.6676 (θ) + 288.66
100	M = 5.0883 (θ) + 579.44
150	M = 5.5090 (θ) + 870.22
200	M = 5.9298 (θ) + 1161.0

3.2.4 Opus90 loop

Fig. 15 is the deformed configuration of Opus90 loop obtained from FEM as compared to Fig. 4 (b). Observe that, since the loop is unsymmetrical, distortion of its shape after activation is more than other types of loops. The ratios of M/F for the anterior and posterior legs when the loop is centered within IBD are 5.36 and 4.48, respectively. Owing to the unsymmetrical nature of the loop, M/F and

moments in the anterior and posterior legs are unequal; the effect of gable bend angles will not be presented herein.

4. Discussion and Conclusion

In this Part II study, FEM is used as a tool to calculate the values of M/F and loop stiffness numerically for four types of closing loops. Experimental verification on the loop stiffness was done on a Lloyd universal testing machine. Comparison of the results, including those presented by Siatkowski [2], is shown in Table VIII. For the vertical helical loops, T-loop and helical T-loop, the loop stiffness obtained by FEM show very good agreement with our experimental findings and those from Siatkowski [2]. For the Opus90 loop, the loop stiffness obtained by FEM shows a rather large discrepancy from experiment, but the difference of M/F is still within acceptable accuracy. Also the ratios of M/F of the Opus90 and T-loop agree rather well with the experimental results. Based on these observations, we, therefore, recommend that orthodontists use the present equations for M/F and moments shown in Table II to VII as the estimated values of the 0.40x0.55 mm stainless steel loop configuration.

Table VIII. Comparison of loop properties to FEM

Loop Type[1]	Finite Element		Experiment	Siatkowski[2]	
	k (gm/mm)	M/F (mm)	k (gm/mm)	k (gm/mm)	M/F (mm)
Vertical Helical	82.88	4.67	81.90	-	-
T-loop	59.50	5.06	59.63	58.80	4.60
Opus90 loop	71.57	5.36[3]	55.94	62.50	5.80[3]
Helical T-loop	49.82	5.82	47.66	-	-

[1]All closing loops are centered within IBD.
[2]Interbracket distance (IBD) of Siatkowski is 13 mm. and present study 14 mm.
[3]M/F of anterior leg when loop is centered within IBD.

5. References

[1] MSC/NASTRAN for Windows, The MacNeal-Schwendler Corporation, U.S.A., 1997.

[2] Siatkowski, R. E. Continuous Arch Wire Closing Loop Design, Optimization and Verification: Part II. Am J Orthod Dentofac Orthop, Vol. 112, pp. 487-495, (November 1997).

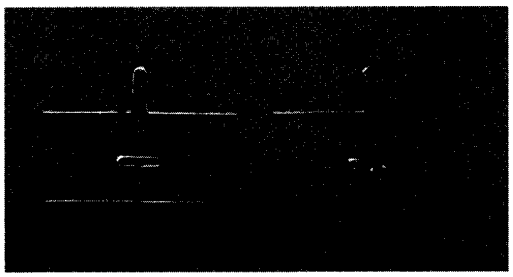

Fig. 1. Sample of four types of closing loops

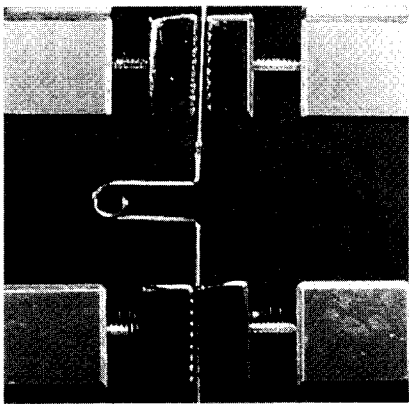

Fig. 2a. Vertical helical loop before activation

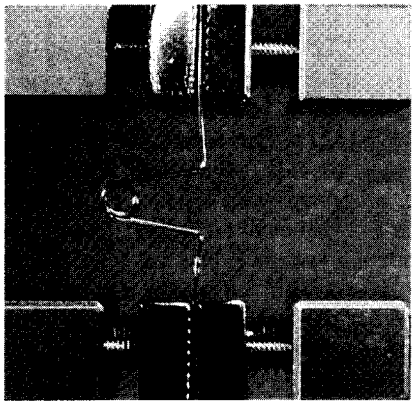

Fig. 2b. Vertical helical loop after 3 mm activation

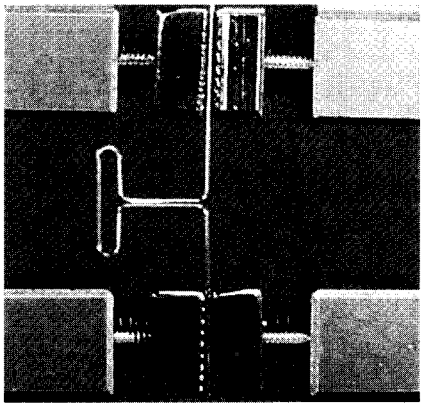

Fig. 3a. T-loop before activation

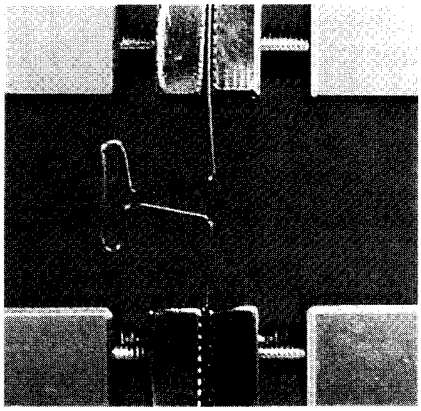

Fig. 3b. T-loop after 3 mm activation

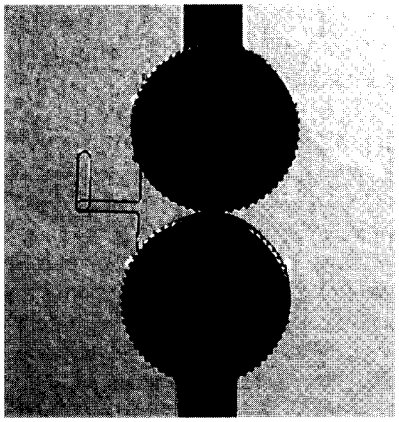

Fig. 4a. Opus90 loop before activation

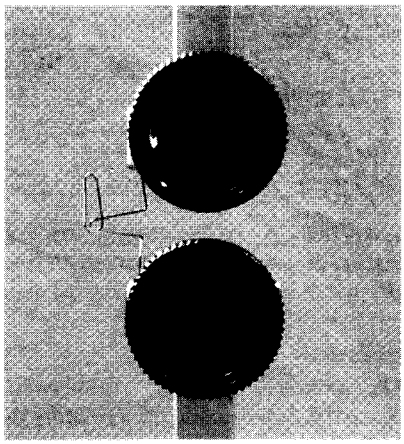

Fig. 4b. Opus90 loop after 3 mm activation

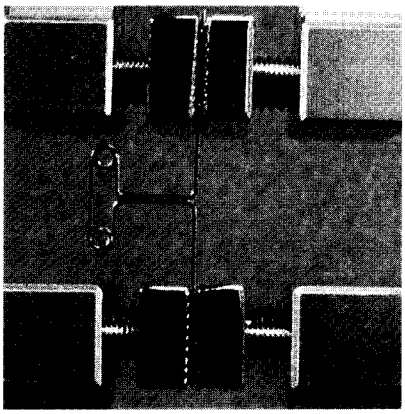

Fig. 5a. Helical T-loop before activation

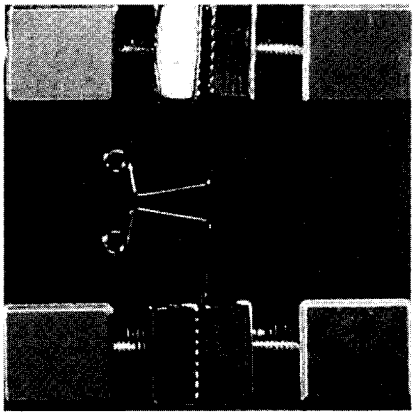

Fig. 5b. Helical T-loop after 3 mm activation

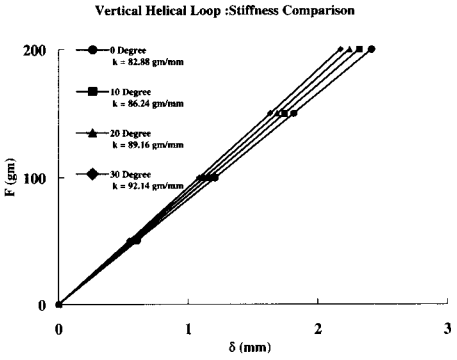

Fig. 8. Effect of gable bends on loop stiffness of vertical helical loop

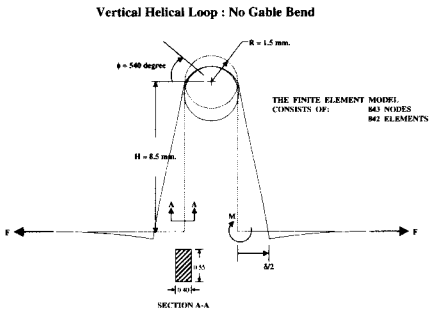

Fig. 6. Deformed configuration of vertical helical loop

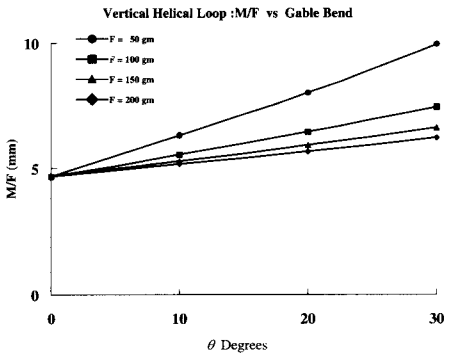

Fig. 9. M/F vs. gable bend angle of vertical helical loop

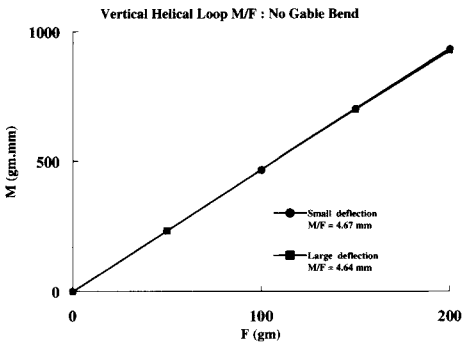

Fig. 7. Moment vs. activating force of vertical helical loop

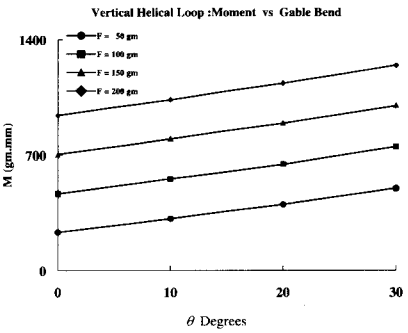

Fig. 10. Moment vs. gable bend angle of vertical helical loop

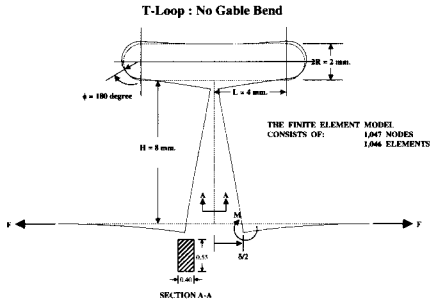

Fig. 11. Deformed configuration of T-loop

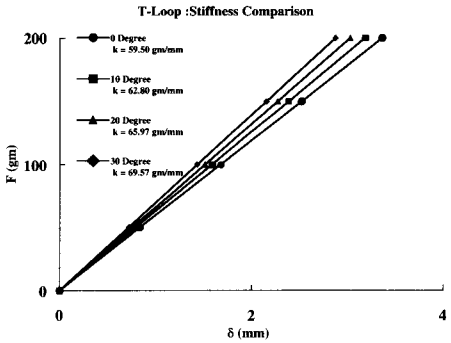

Fig. 12. Effect of gable bends on loop stiffness of T-loop

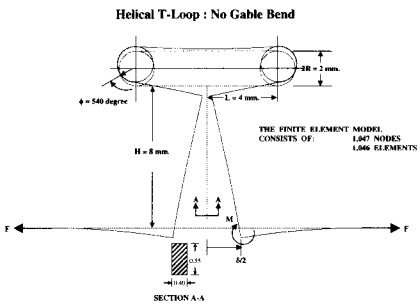

Fig. 13. Deformed configuration of helical T-loop

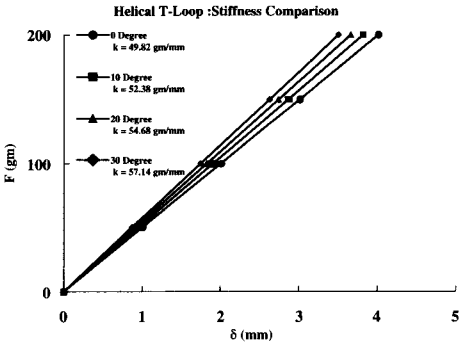

Fig. 14. Effect of gable bends on loop stiffness of helical T-loop

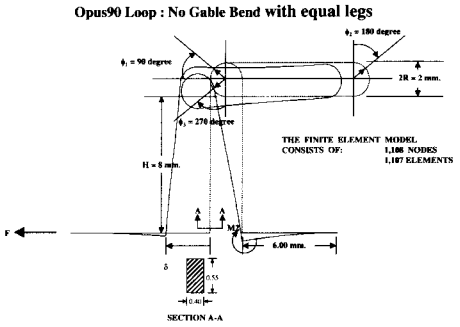

Fig. 15. Deformed configuration of Opus90 loop